



**HAL**  
open science

## Asphaltene Agglomeration Through Physical-Chemical and Rheological Testing

Rodrigo Shigueiro Siroma, Mai Lan Nguyen, Pierre Hornych, Jean-Pascal Planche, Jeramie Adams, Joseph Rovani, Yogesh Kumbargeri, Yvong Hung, Aurélia Nicolai, Layella Ziyani, et al.

► **To cite this version:**

Rodrigo Shigueiro Siroma, Mai Lan Nguyen, Pierre Hornych, Jean-Pascal Planche, Jeramie Adams, et al.. Asphaltene Agglomeration Through Physical-Chemical and Rheological Testing. Road Materials and Pavement Design, 2023, pp.1-14. 10.1080/14680629.2023.2221744 . hal-04370191

**HAL Id: hal-04370191**

**<https://hal.science/hal-04370191>**

Submitted on 2 Jan 2024

**HAL** is a multi-disciplinary open access archive for the deposit and dissemination of scientific research documents, whether they are published or not. The documents may come from teaching and research institutions in France or abroad, or from public or private research centers.

L'archive ouverte pluridisciplinaire **HAL**, est destinée au dépôt et à la diffusion de documents scientifiques de niveau recherche, publiés ou non, émanant des établissements d'enseignement et de recherche français ou étrangers, des laboratoires publics ou privés.



Distributed under a Creative Commons Attribution - NonCommercial - NoDerivatives 4.0 International License

## **Taylor & Francis Word Template for journal articles**

Rodrigo Shigueiro Siroma<sup>a\*</sup>, Mai Lan Nguyen<sup>a</sup>, Pierre Hornych<sup>a</sup>, Jean-Pascal Planche<sup>b</sup>, Jeramie Adams<sup>b</sup>, Joseph Rovani<sup>b</sup>, Yogesh Kumbargeri<sup>b</sup>, Yvong Hung<sup>c</sup>, Aurélia Nicolai<sup>d</sup>, Layella Ziyani<sup>e</sup>, and Emmanuel Chailleux<sup>a</sup>

*<sup>a</sup>Materials and Structures Department, Université Gustave Eiffel, Bouguenais, France;*

*<sup>b</sup>Western Research Institute, Laramie/Wyoming, United States; <sup>c</sup>TotalEnergies, Solaize,*

*France; <sup>d</sup>Spie Batignolles Malet, Portet-sur-Garonne, France; <sup>e</sup>École Spéciale des*

*Travaux Publics, du Bâtiment et de l'Industrie, Cachan, France*

Corresponding author's e-mail address: [rodrigo-shigueiro.siroma@univ-eiffel.fr](mailto:rodrigo-shigueiro.siroma@univ-eiffel.fr);

[rodrigo\\_siroma@yahoo.com](mailto:rodrigo_siroma@yahoo.com)

# Asphaltene Agglomeration Through Physical-Chemical and Rheological Testing

Binder aging has long been recognized as one of the key factors behind several types of pavement distresses. A better understanding of the changes in binder chemistry and microstructure triggered by aging is fundamental as they increase the cracking susceptibility of asphalt materials and reduce pavement durability, one of its main life-cycle cost analysis (LCCA) drivers. In this context, this paper presents the findings of a collaborative study that delves further into the alterations in binder chemistry, microstructure, and rheology of laboratory- and field-aged binders using innovative experimental and fundamental theory techniques developed by partner teams. An increase in polarity leading to a shift in the apparent molecular weight distribution (AMWD) towards higher molecular weights, which implies molecular agglomerations, could be observed as a result of oxidation via Saturates, Aromatics, Resins, and Asphaltene Determinator (SAR-AD) and Size Exclusion Chromatography (SEC), respectively. As for the theoretical methods, the  $\delta$ -method and Molecular Agglomeration Index (MAI) estimate the AMWD and incidence of molecular agglomeration, respectively, solely from binder rheology. Both methods show satisfactory relationship with the SAR-AD and SEC results. This reinforces the soundness of the  $\delta$ -method and MAI.

Keywords: Asphalt binder; aging; rheology; binder composition; molecular weight distribution

## 1 Introduction and Background

Asphalt binder is a complex hydrocarbon product that corresponds to the heaviest fraction obtained from the distillation of crude oil during refining whose composition is highly dependent on the crude oil source, refining processes, and aging (Branthaver et al., 1993; Hunter et al., 2015). The broad range of molecular types that compose asphalt binders interacting together is what provides binders with unique properties. However, due to the high complexity of the binder's chemical composition, binders have

traditionally been fractionated into two broad groups called maltenes (saturates, aromatics, and resins) and asphaltenes in terms of solubility (Corbett, 1969).

Asphaltenes are the most polar fraction and therefore the structuring entity. In the literature, several molecular weight values can be found for asphaltenes depending on the methods and testing conditions. The significant advances in analytical chemistry, especially in mass spectrometry, enable more accurate estimations of the asphaltene molecular weight. Hence, (Mullins, 2011) stated that the average molecular weight for a single asphaltene molecule obtained by Time-Resolved Fluorescence Depolarization (TRFD) is approximately 750 g/mol, varying from 500 to 1,000 g/mol.

This highly complex chemical composition induces spatial organization and arrangement of molecules impacting directly the binder overall mechanical behavior. Among the several models presented in the literature, the colloidal model has remained the most accepted and successful in describing binder structure, although some important aspects remain to be understood. In this model, binder is regarded as a colloidal system consisting of high molecular weights asphaltene micelles dispersed in a maltenic phase (lower molecular weight oily medium). These asphaltene micelles are peptized by aromatic resins that act as a stabilizing solvation shell in an oily medium, and thus preventing aggregation. (Pfeiffer & Saal, 1940) proposed two binder structural arrangements to explain the difference in rheological properties of two very distinguished binders called sol and gel. Sol-type binders display Newtonian behavior as they have enough aromatics and resins to completely solvate and peptize the asphaltene molecules. In contrast, if the amounts of aromatics and resins are insufficient, the asphaltene micelles can get fully interconnected, thus reducing asphaltene micelles' mobility within the binder and consequently resulting in a non-

Newtonian behavior. Most binders are found to have an intermediate behavior between sol- and gel-type binders.

A better understanding of asphaltene agglomeration is therefore of utmost importance as asphaltenes play a major role in many physical and chemical properties of binders. In the early 1960s, (Yen et al., 1961) proposed a model of a colloidal system formed by units composed of polycondensed aromatic rings substituted by aliphatic chains and naphthenic polycyclic rings through X-Ray Diffraction (XRD). Through the advances in asphaltene science, (Mullins, 2010) proposed the Modified Yen, or Yen-Mullins, model that proposes three asphaltene hierarchical structures: asphaltene monomers, nanoaggregates with an aggregation number of around six, and clusters consisting of eight nanoaggregates.

To ensure optimum pavement serviceability and durability, an asphalt binder must meet a set of several specifications—most of them rheology-based (Anderson & Kennedy, 1993; Lesueur et al., 2021). Hence, any significant alteration in rheological behavior that may take place over service time is usually undesirable because this indicates reduced asphalt material performance and, consequently, faster deterioration of roadways. However, these changes are likely to happen due to the organic nature of asphalt binder that makes it highly prone to oxidative aging when in contact with oxygen in the air. Oxidation increases the concentration of polar functional groups and pericondensed aromatic molecular structures which favor intermolecular agglomeration (Boysen & Schabron, 2015; Petersen, 2009). This reduces the mobility between molecules and, consequently, causes binders to stiffen and embrittle, thus impairing the binders' ability to dissipate mechanical and thermal stresses. The accumulation of these irreversible changes triggered by binder aging over the years in service shortens the durability of pavements as they become more susceptible to cracking.

A better understanding of how the binder chemistry and microstructure change, and the consequences thereof, is of utmost importance for designing longer-lasting roads and more cost-effective maintenance strategies. For this purpose, this paper presents the findings regarding the assessment of asphaltene molecular association through innovative theoretical and experimental methods. In this case, the composition and microstructure of four laboratory- and field-aged binders were characterized via Saturates, Aromatics, Resins, and Asphaltene Determinator (SAR-AD) and Size Exclusion Chromatography (SEC), respectively. The rheological measurements were performed through Dynamic Shear Rheometer (DSR) and Metravib Dynamic Mechanical Analysis (DMA). Finally, the rheological measurements were used to estimate the apparent molecular weight distribution (AMWD) and incidence of asphaltene molecular agglomeration through the  $\delta$ -method and Molecular Agglomeration Index (MAI), respectively.

## **2 Experimental Methods**

### **2.1 Materials**

Four unmodified 35/50 pen grade binder samples were rigorously characterized. Two of them were from the same supply batch of a binder grade widely used in road construction in France (binder A) conditioned at different aging levels: fresh (binder A\_Fr) and laboratory-aged through Rolling Thin-Film Oven (RTFO) followed by 20 hours of Pressure Aging Vessel (PAV) (binder A\_1P). The two other binders were extracted and recovered from class 3 'Grave Bitume (GB3)' mixes present in the bottommost layer of the asphalt course base (ACB) located in the trafficked zones of two thick pavement sites in France: the Test Track B of the Université Gustave Eiffel (UGE)'s Fatigue Carrousel in Nantes (western France) and RD14 departmental road

near Montpellier (southern France). The UGE's Test Track B was built in 1998 and the pavement structure consists of an 8 cm asphalt wearing course, and its ACB consists of a 6 cm asphalt base layer built on two identical asphalt base layers of 15 cm each. As for RD14 road built in 2005, its structure consists of a 6 cm asphalt wearing course and a 8 cm base layer. The binders from Nantes and Montpellier are named NF3T and MB1T, respectively, and their respective base layers investigated in this study are represented in red in Figure 1.

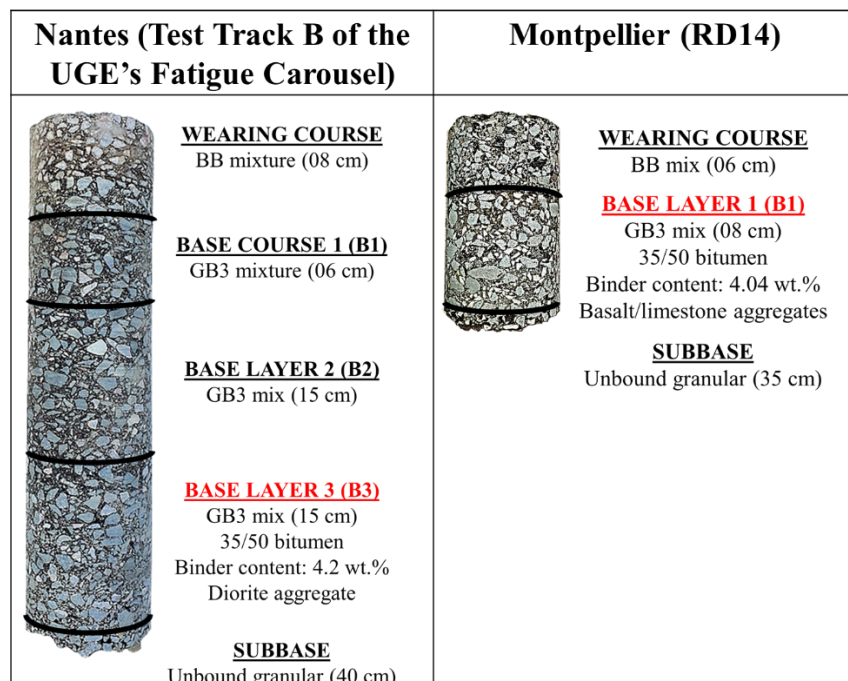


Figure 1. Pavement structures of the field sections in Nantes and Montpellier and the base layer (in red) from which the field-aged binders were extracted and recovered.

## 2.2 Experimental Methods

### 2.2.1 Saturates, Aromatics, Resins, and Asphaltene Determinator (SAR-AD)

SAR-AD method is an automated separation developed by the Western Research Institute (WRI) and performed on High Performance Liquid Chromatography (HPLC)

equipment that is capable of providing hundreds of separations without regenerating column packing materials (Boysen & Schabron, 2015). For this separation, the asphalt binder samples were initially dissolved into chlorobenzene and then filtered with a 0.45  $\mu\text{m}$  syringe filter to form 20  $\mu\text{L}$  of 10 wt/vol % binder solutions. With this method, the binder is separated into eight constituent fractions: saturates, aromatics 1, aromatics 2, aromatics 3, resins,  $\text{C}_7\text{C}_6$ -asphaltenes, toluene-asphaltenes, and  $\text{CH}_2\text{Cl}_2$ -asphaltenes. Further information on each SAR-AD fraction can be found in (Adams et al., 2019, 2021). Peak elution is detected with an evaporative light scattering detector (ELSD), which provides an approximate weight percent of the fraction, and an optical absorbance detector at 500 nm, which determines the concentration of brown-colored pericondensed aromatic content of each fraction. For the initial stage of the separation the asphaltenes precipitate from the injected solution onto a ground polytetrafluoroethylene (PTFE) packed column charged with excess of heptane. The precipitated asphaltenes are further separated based on their solubility using solvents of increasing solvent strength (or solubility parameter): cyclohexane ( $\text{C}_6\text{H}_{12}$ ), toluene, and methylene chloride: methanol ( $\text{CH}_2\text{Cl}_2$ ) The heptane soluble maltenes are then separated by chromatography on three different sorbents to provide the saturates, aromatics 1, aromatics 2, aromatics 3 and resins fractions.

WRI developed indices based on the measurements using both ELS and 500 nm detectors. Polarity/Coking Index is the ratio of the  $\text{C}_7\text{C}_6$ -soluble asphaltenes to the  $\text{CH}_2\text{Cl}_2$ -soluble asphaltenes (both 500 nm peak areas) and quantifies the pyrolysis/thermal severity history during refining. A higher coking index is conventionally desirable and values below 1 typically indicate the presence of coke (an undesirable product from thermal or catalytic cracking for upgrading petroleum residues). Absorbance Aging Index (AAI) is the ratio of the toluene-soluble asphaltenes

500 nm peak area to the sum of aromatics 2, aromatics 3, and resins 500 nm peak areas. This measures the aging level of the binder as it increases with aging. Total Pericondensed Aromaticity (TPA) has also been used to estimate the aging level and is the division of the total asphaltenes ELS peak areas by the sum of the total asphaltenes 500 nm peak areas, which quantifies the amount of pericondensed aromatic structures that absorb visible light and are believed to be viscosity builders due to their high polarity (Schabron & Rovani, 2008). Finally, the Colloidal Instability Index (CII), which is already commonly used as a stability index, is the ELSD peak ratio for the sum of the incompatible saturates, aromatics 1, and total asphaltenes to the sum of the asphaltene dissolving and dispersion fraction of aromatics 2, aromatics 3, and resins. The CII value increases with aging or for asphalts that have a poorly balanced composition by having very high saturates or asphaltenes, or both.

### 2.2.2 *Size Exclusion Chromatography (SEC)*

SEC was conducted in an Agilent 1260 Infinity II HPLC instrument to determine the apparent molecular weight distribution (AMWD) of the binder samples. Sigma-Aldrich's tetrahydrofuran (THF  $\geq 99.9$ , inhibitor-free) was used for the mobile phase with a flow rate of 3.5 mL/min. Each binder sample was diluted in THF at a concentration of 0.1 g/mL and filtered with a 0.45  $\mu\text{m}$  syringe filter. 7.5  $\mu\text{L}$  of the binder solutions were then injected into a Waters  $\mu$ -styragel HR2 column (30 cm x 7.5 mm i.d.) packed with 5  $\mu\text{m}$  particles at a constant temperature of 30°C. SEC detection was achieved using an ELSD and a variable wavelength optical absorbance detector set at 500 nm, 400 nm, 350 nm, 300 nm, 280 nm, and 250 nm. The calibration curve was obtained with polystyrene standard samples with MW values of 254, 1,890, and 13,000 g/mol.

### 2.2.3 Rheological Measurements

Temperature-frequency sweep testing was performed within the linear viscoelastic regime on two different instruments: Dynamic Shear Rheometer (DSR) and Metravig Dynamic Mechanical Analysis (DMA). DSR was performed on a Malvern Kinexus instrument with a 4 mm (-30°C to 30°C) and 8 mm (30°C to 60°C) diameter parallel plates, at frequencies varying from 0.0159 to 15.92 Hz (0.1 to 100 rad/s). Unlike DSR, the rheological measurements conducted in a Metravig DMA rheometer were in tension-compression mode ( $E^*$ ) at low temperatures, from -15 to 20°C, and annular shear mode ( $G^*$ ) at high temperatures, from 20 to 60°C, at 1–80 Hz (6.28 to 502.65 rad/s). The conversion between  $|G^*|$  and  $|E^*|$  was made considering a Poisson's ratio of 0.5. The shift factors ( $a_T$ ) for each experimental isotherm to build the master curves were computed through the mathematical-based method (Chailleux et al., 2006) that is based on the Kramer-Kronig relation between the real and imaginary components of complex functions (Booij & Thoone, 1982) as presented in Equation 1:

$$\log(a_{T(T_i, T_{ref})}) = \sum_{j=1}^{j=ref} \frac{\log(|E^*(T_j, \omega)|) - \log(|E^*(T_{j+1}, \omega)|)}{\varphi_{avg}[(T_j, T_{j+1}), \omega]} \quad (1)$$

where  $a_{T(T_i, T_{ref})}$  is the shift factor of an isotherm corresponding to  $T_i$  in relation to  $T_{ref}$ ,  $|E^*(T_j, \omega)|$  is the complex modulus norm at a given temperature  $T_j$  and frequency  $\omega$ , and  $\varphi_{avg}$  is the mean value of the phase angles at  $T_j$  and  $T_{j+1}$ , both at frequency  $\omega$ . The Williams-Landel-Ferry (WLF) (Williams et al., 1955) law's coefficients were also calculated.

The 2 Springs, 2 Parabolic elements, and 1 Dashpot (2S2P1D) rheological model (Olard & Di Benedetto, 2003) was used to fit the raw data, considering the static modulus ( $E_0$  or  $G_0$ ) equals 0 for binders, and is given by Equation 2:

$$E^*(i\omega\tau) = E_0 + \frac{E_\infty - E_0}{1 + \delta(i\omega\tau)^{-k} + (i\omega\tau)^{-h} + (i\omega\beta\tau)^{-1}} \quad (2)$$

where  $i$  is the imaginary unit,  $\omega$  is the frequency in radian per second,  $E_\infty$  is the glassy modulus,  $\delta$  is the dimensionless calibration constant,  $k$  and  $h$  are the ratio  $E_{\text{imag.}}/E_{\text{real}}$  when  $\omega$  tends to 0 and  $\infty$ , respectively,  $\beta$  represents the Newtonian viscosity, and  $\tau$  is the characteristic time. These parameters are determined through mathematical optimization that reduces as much as possible the differences between the modeled and experimental data.

Since the rheology-based theoretical approaches employed in this study are solely based on the phase angle master curve, it is worth mentioning the approximated analytical equation (Equation 3) proposed by (Krolkral et al., 2018) to compute the phase angle derived from the 2S2PID equation considering the (Booij & Thoone, 1982) approximation:

$$\varphi(\omega) \approx \frac{\pi}{2} \cdot \left[ \frac{k \cdot \delta(\omega\tau)^{-k} + h(\omega\tau)^{-h} + (\beta\omega\tau)^{-1}}{1 + \delta(\omega\tau)^{-k} + (\omega\tau)^{-h} + (\beta\omega\tau)^{-1}} \right] \quad (3)$$

### 2.3 Theoretical Methods

In the past few years, a theoretical method based on (Zanzotto et al., 1999)'s findings has been developed to propose an “inverse approach” to determine the AMWD of a given asphalt binder based on its linear viscoelastic behavior: the  $\delta$ -method. One of the motivations behind this “inverse approach” was to circumvent some shortcomings of classical SEC such as its premise of significantly reducing associations, some of which likely resulted from processes triggered by aging, and thus preventing potential insights that could be gained into changes in the microstructure of binders with aging. In this

case, the AMWD obtained via SEC may not correspond to the microstructure of the bulk, or undiluted, binder.

### 2.3.1 $\delta$ -method

The  $\delta$ -method was initially inspired by the reported satisfactory sensitivity of the  $|G^*|$  to the AMWD stated in previous works in polymers science (Tuminello, 1986; Tuminello & Cudré-Mauroux, 1991); however, unlike polymers, the phase angle (that was referenced by the Greek letter “ $\delta$ ” in (Zanzotto et al., 1999)) appears to be the most sensitive rheological parameter for estimating the AMWD of asphalt binder.

Considering that binder can be portrayed as a mixture of monodisperse molecular weight species where each molecule has a unique relaxation frequency below which this molecule is relaxed, i.e., does not contribute to the overall mechanical resistance, two scenarios can be observed: at low frequencies (or high temperatures), only apparently large molecules contribute to the overall resistance and thus generating decreased modulus and increased phase angle; and at high frequencies (or low temperatures) where not only large molecules but also small ones contribute to the binder’s mechanical resistance and thereby increasing the modulus and reducing phase angle. Using several binders from the Strategic Highway Research Program (SHRP) library and some Alberta crude oils, (Zanzotto et al., 1999) establish a relation between the crossover frequency ( $\omega_c$ ) at  $T_{ref}=0^\circ\text{C}$  and the molecular weight obtained from Vapor Pressure Osmometry that is expressed by Equation 4:

$$\log(MW) = 2.880 - 0.06768 * \log(\omega_c) \quad (4)$$

Following up (Zanzotto et al., 1999), (Themeli et al., 2015) stated that the Cumulative Molecular Weight Distribution (CMWD) was proportional to the phase angle master curve ( $\delta$ ) and was given by Equation 5:

$$CMWD = \frac{1}{90^\circ} \delta(MW) \quad (5)$$

The derivative of the CMWD finally resulted in the AMWD as shown in Equation 6:

$$AMWD = \frac{d(CMWD)}{d[\log(MW)]} \cong \frac{\Delta(CMWD)}{\Delta[\log(MW)]} \quad (6)$$

Where a differential step size of 1/3,000 was suggested in (Themeli et al., 2016). It is worth mentioning an analytical equation to determine AMWDs that takes into consideration only the rheological parameters of the 2S2P1D model proposed by (Krolkral et al., 2018).

### 2.3.2 Molecular Agglomeration Index (MAI)

Aiming to delve further into the potential of phase angle master curve relationships with multivariate statistical analyses such as Principal Component Analysis (PCA) and Hierarchical Cluster Analysis (HCA), (Siroma et al., 2021) it was found that with aging the most relevant change in phase angle master curve at 0°C reference temperature takes place at approximately  $5.7 \times 10^{-6}$  Hz. This finding led ( Siroma et al., 2022) to revisit the  $\delta$ -method so that the observed reduced frequency value corresponds to molecular sizes of approximately 1,700 g/mol. A follow-up study with a more robust data set allowed updating the most relevant reduced frequency value to  $8.5 \times 10^{-6}$  Hz, which corresponds to approximately 1,500 g/mol. In the petroleum research world, it is

admitted that asphaltene molecules have an average molecular weight of about 500-800 g/mol (Mullins, 2011), so this threshold would correspond to the association of approximately two to three asphaltene molecules. Consequently, ( Siroma et al., 2022) proposed a new index to quantify the asphaltene agglomeration named Molecular Agglomeration Index (MAI). MAI consisted of dividing the area below the AMWD curve above 1,500 g/mol by the total area and varies from 0 to 1, where the closer to 1 the greater the incidence of agglomerated molecules, as shown in Equation 7 and illustrated in Figure 2:

$$MAI = \frac{\text{Area above 1,500 g/mol } (A_{1,500})}{\text{Total are } (TA)} \quad (7)$$

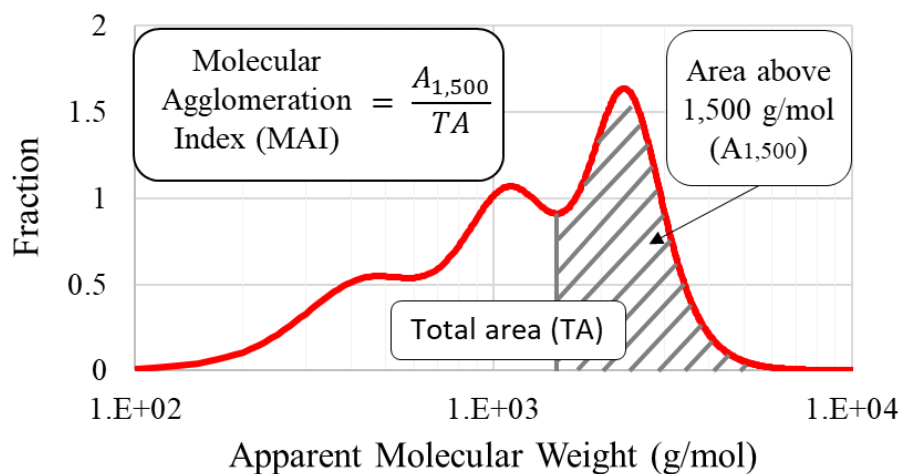


Figure 2. Molecular Agglomeration Index (MAI)

As stated by (Petersen, 1984), the delicate balance, or the lack of it, between associated or agglomerated components and dispersed or solubilized components strongly impacts the performance of asphalt binders. MAI increases with aging, where a threshold value of 0.58 was proposed as a failure criterion that is in agreement with the

three binder-based rheological failure criteria presented in subsection 2.4. It is worth mentioning that MAI is a shape parameter since it takes into account the entire phase angle master curve.

## ***2.4 Rheology-based failure criteria***

Rheology has proven to be a powerful tool to assess binder durability as it is the backbone of some current performance-related binder specifications. Furthermore, some thresholds based on the linear viscoelastic behavior of binders found in cracked zones of roadways have been proposed over the years to indicate a possible critical point for maintenance, i.e., the state from which asphalt materials are more susceptible to degradation.

### *2.4.1 Glover-Rowe (G-R) parameter*

The intermediate temperature G-R criterion (Rowe, 2011) has widely been used to evaluate the non-load cracking performance of asphalt materials. The G-R combines the effect of stiffness (complex modulus  $|G^*|$ ) and viscoelasticity (phase angle  $\varphi$ ) and is expressed as follows:

$$G - R = \frac{|G^*|(\cos \varphi)^2}{(\sin \varphi)} \quad (8)$$

where  $|G^*|$  and  $\varphi$  are calculated at 15°C and 0.005 rad/s. (Rowe, 2011) proposed that the damage onset and significant cracking susceptibility due to non-load-related cracking were likely to arise when G-R was higher than 180 kPa and 600 kPa, respectively.

#### 2.4.2 *Limiting temperatures corresponding to the 27° and 45° phase angles*

Among the rheological parameters employed in several surveys conducted in the 1990s on several French roads after 7 years of service (Groupe National Bitume, 1999), the temperatures corresponding to the phase angles of 27° and 45° at 7.8 Hz of the extracted and recovered binders presented one of the best correlations with the cracking incidence on the surface of the studied sections. Further discussion on both criteria can be found in ( Siroma et al., 2022). Both temperatures increase with aging and limiting values of  $T_{(\varphi=27^\circ)} = 12^\circ\text{C}$  and  $T_{(\varphi=45^\circ)} = 35^\circ\text{C}$ , both at 7.8 Hz, were settled for unmodified 35/50 pen grade binders.

### 2.5 *Results*

#### 2.5.1 *Chemical and microstructure changes*

The percent of each SAR-AD fraction and some indices are summarized in Table 1. The RTFO+PAV aging condition on fresh control A\_Fr results in a reduction of aromatics (mainly in aromatics 2 and 3) and an increase in asphaltenes (more marked in the toluene-soluble asphaltenes). The saturates and resins contents remained practically unchanged. Depending on the binder and aging level, it can be seen positive or negative net production of resins as it is a transition fraction from aromatics to asphaltenes.

According to the coking index, the binders do not appear to have undergone thermal or catalytic cracking and the presence of coke is unlikely, even though a slight reduction in the coking index value can be observed for A\_1P. As for the aging indices, the AAI, TPA, and CII increase when A\_Fr is subjected to accelerated laboratory aging conditions. According to these SAR-AD aging indices, the four binders can roughly be ranked, from least to most aged, as following: A\_Fr, NB3T, MB1T, and A\_1P.

Depending on the aging indice, binder MB1T does not follow the aforementioned rank since it displays the highest TPA value and its AAI is the second lowest one.

Table 1. SAR-AD results.

Detector	A_Fr		A-1P		NB3T		MB1T	
	ELS	500 nm						
<b>Saturate</b>	11.70	-	12.07	-	9.86	-	11.13	-
<b>Aromatics 1</b>	6.07	-	6.27	-	5.66	-	5.19	-
<b>Aromatics 2</b>	20.58	0.2	18.88	0.16	18.75	0.18	15.55	0.18
<b>Aromatics 3</b>	36.44	17.36	31.53	13.18	34.94	15.61	32.94	14.28
<b>Total Arom.</b>	63.09	-	56.68	-	59.35	-	53.68	-
<b>Resins</b>	11.44	20.24	11.67	15.52	13.64	19.00	16.67	20.77
<b>C<sub>7</sub>C<sub>6</sub> asph.</b>	2.81	13.48	3.57	13.01	3.54	13.89	4.10	14.67
<b>Toluene asph.</b>	10.73	46.59	15.69	55.96	13.40	49.55	14.13	48.14
<b>CH<sub>2</sub>Cl<sub>2</sub> asph.</b>	0.23	2.13	0.32	2.17	0.22	1.78	0.27	1.97
<b>Total Asph.</b>	13.77	-	19.58	-	17.15	-	18.51	-
<b>Coking Index</b>	-	6.34	-	5.99	-	7.78	-	7.45
<b>AAI</b>	-	1.23	-	1.94	-	1.42	-	1.37
<b>TPA</b>	22.14	-	27.53	-	26.30	-	28.57	-
<b>CII</b>	0.46	-	0.61	-	0.49	-	0.53	-

Figure 3 presents all the AMWD curves of control binder A\_Fr obtained via SEC with ELSD and optical absorbance detector at 500 nm, 400 nm, 350 nm, 300 nm, 280 nm, and 250 nm. The shift of the AMWD curve towards higher molecular weights with increasing wavelength shows that the longer the wavelength, the heavier the molecules captured during the measurements at the expense of smaller ones. Since the higher the detection wavelength the more percondensed the molecules, this multiwavelength detection allows to also link the molecular weight to the chemical

structure. Therefore, three AMWD curves encompassing the most diverse molecules that make up binder will be used to compare the four studied binders as shown in Figure 4: ELSD (left), and optical absorbance detector at 500 nm (middle) and 350 nm (right).

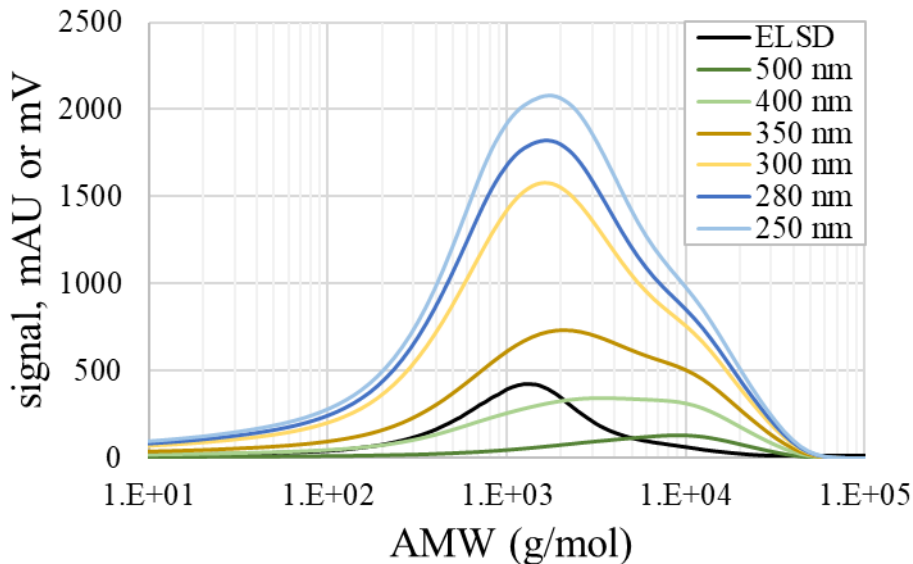


Figure 3. All the SEC AMWD of control binder A\_Fr

According to WRI's previous works, ELSD is sensitive to detecting all different binder fractions. ELSD curves for all the binders are quite similar: a unimodal-shaped curve centered at approximately 1,100 g/mol with a slight divergence in high molecular masses where the AMWD of control binder A\_Fr is lower than those of the three other binder samples. On the other hand, measurements with the optical detector at 500 nm are more sensitive to the highly conjugated aromatic molecules such as asphaltenes with a minor contribution from resins. Resembling a negative-skewed distribution curve with a shoulder at approximately 10,000 g/mol, the peak of the 500 nm AMWD curves increases with aging and this trend is in line with the SAR-AD results. 350 nm AMWD is more adequate to detect the aromatics content in aromatics 2, aromatics 3, resins, and asphaltenes. In this case, the AMWD curves display two peaks that increase with aging.

NB3T and MB1T are in between A\_Fr and A\_1P, which is in line with the overall trend observed with the SAR-AD results. Note these high values are typical of apparent molecular weight (MW) and confirm the high degree of molecular association that can occur particularly after aging. This also shows that the SEC solvent does not destroy all molecular associations. The high MW shoulders show that associations grow upon aging both for asphaltenes and more polar/aromatic maltenes.

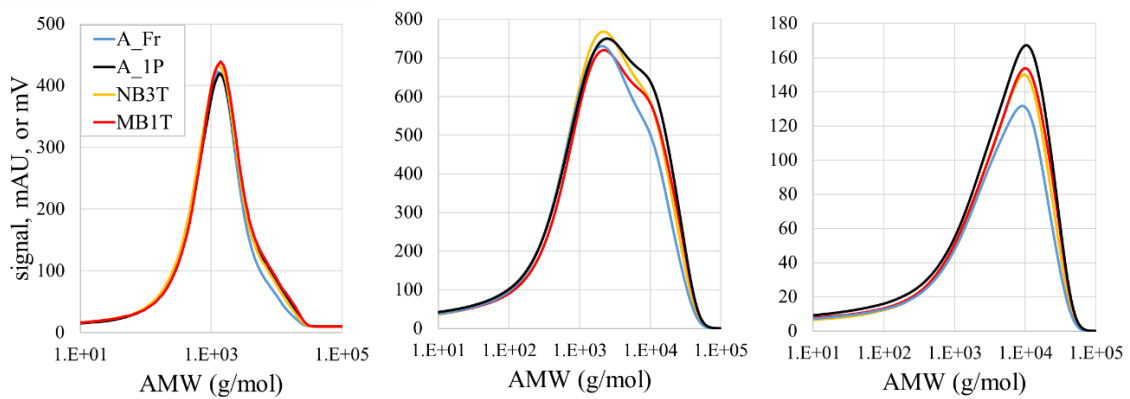


Figure 4. SEC AMWD with ELSD (left) and optical absorbance detector at 350 nm (middle) and 500 nm (right).

### 2.5.2 Rheological testing results

Although different rheometers with significantly different settings and solicitation modes (shear vs. traction/compression) have been used in this work, the experimental raw data obtained with 4-mm- and 8-mm-DSR and the respective 2S2P1D parameters (Table 2) and fitted curves correspond satisfactorily with those obtained with Metravig DMA for all the binder samples. Figure 5 shows a good match between the phase angle master curves and the  $\delta$ -method AMWDs of all the four binders obtained from both measurements.

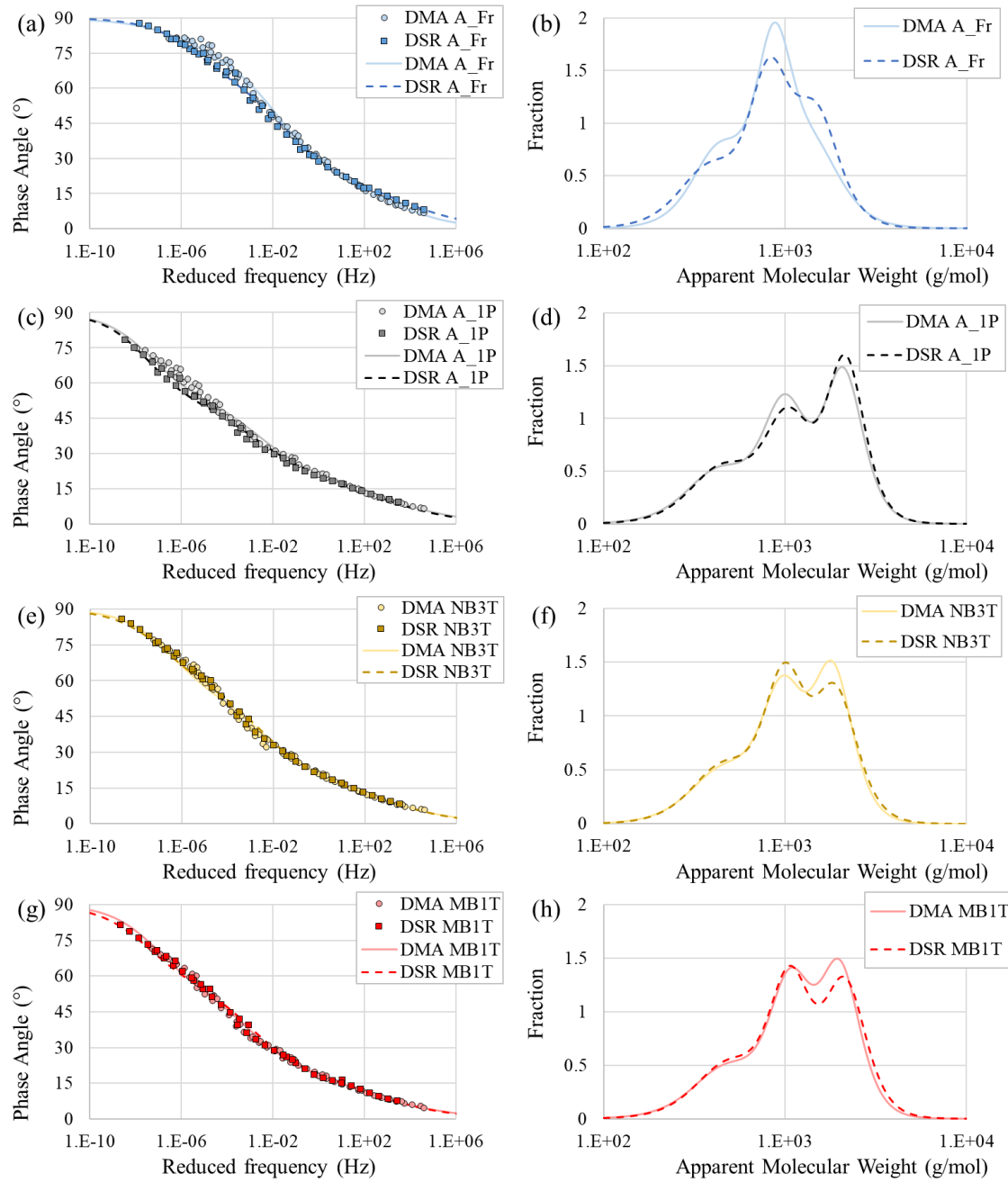


Figure 5. (a), (c), (e), and (g) represent the phase angle master curves obtained with Metravib DMA and DSR rheometers of binders A\_Fr, A\_1P, NB3T, and MB1T, respectively, and (b), (d), (f), and (h) are their corresponding  $\delta$ -method AMWDs.

Table 2. 2S2P1D and WLF parameters at  $T_{ref} = 0^{\circ}\text{C}$  obtained for all the binders characterized with Metravib DMA and DSR rheometers ( $E_{\infty}$  in MPa).

Binder	Device	2S2P1D rheological model						WLF model	
		$E_{\infty}$	$\delta$	$k$	$h$	$\beta$	$\tau$	C1	C2
A_Fr	DMA	2183	5.94	0.30	0.71	32.4	0.094	20.46	127.7
	DSR	2299	5.74	0.26	0.65	111.6	0.033	26.56	167.3
A_1P	DMA	2426	6.01	0.24	0.60	684.0	0.363	25.23	152.8
	DSR	2015	5.96	0.25	0.58	880.6	0.509	30.03	195.9
NB3T	DMA	2313	5.13	0.24	0.60	274.6	0.412	26.25	158.4
	DSR	2406	5.70	0.25	0.63	203.7	0.537	31.19	199.9
MB1T	DMA	2255	5.68	0.24	0.60	273.1	1.434	26.73	161.5
	DSR	2280	5.67	0.24	0.62	308.5	1.444	34.83	228.7

Figure 6 illustrates the phase angle master curves of the four binders and their corresponding AMWD derived from the  $\delta$ -method. The more aged the binder, the lower its phase angle master curve, indicating an increasingly elastic and less viscous material. The phase angle master curves of A\_1P and MB1T overlap reasonably well with each other at high frequencies and/or low temperatures; however, at low frequencies and/or high temperatures, i.e., conditions under which asphalt binder would display a more viscous-like behavior, it can be seen that the phase angle values of binder A\_1P are lower than those corresponding to MB1T. The  $\delta$ -method AMWDs are also portrayed in Figure 6. Control binder A\_Fr presents a unimodal distribution-shaped AMWD with one shoulder on each side, where the left is higher, and centered at around 1,000 g/mol. With aging, the AMWD is shifted towards higher molecular weights and a new peak at approximately 2,000 g/mol emerges. This is believed to represent a new molecular

population that is widely seen in SEC corresponding to asphaltene molecular agglomeration (Adams et al., 2019; Krolkral et al., 2018; Themeli et al., 2015, 2016).

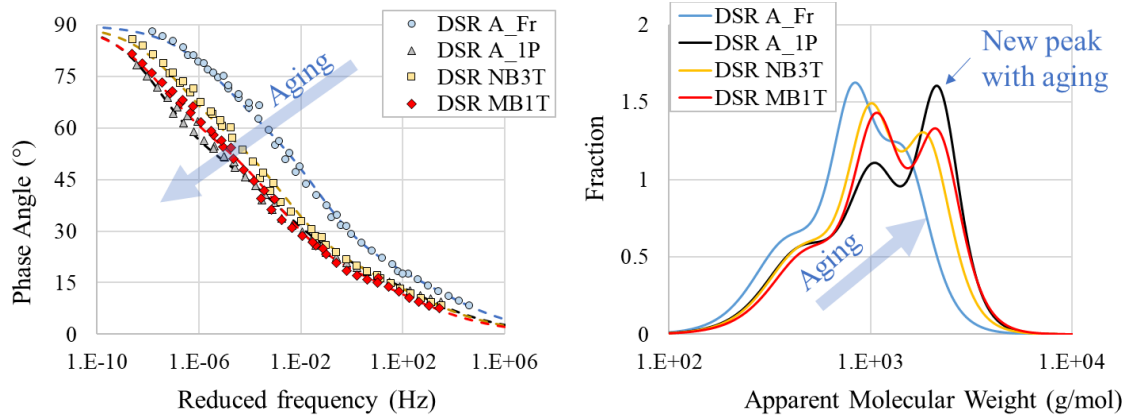


Figure 6. Phase angle master curves (left) and  $\delta$ -method AMWDs (right) obtained from the measurements performed with DSR.

The G-R, MAI,  $T_{(\delta=27^\circ)}$  at 7.8 Hz, and  $T_{(\delta=45^\circ)}$  at 7.8 Hz as well as their standard deviation error bars were computed using the experimental data obtained with Metravib DMA and DSR rheometers and presented in Figure 7. A\_Fr passes all the failure criteria; binder A\_1P, on the other hand, fails in all criteria. As for the field-aged binders, NB3T is classified as a binder with an increased cracking susceptibility according to MAI and MB1T fails in all failure criteria. The variability of the values of these four failure criteria that were calculated from experimental data measured with significantly different rheometers was investigated through the coefficient of variation (CoV) and it is summarized in Table 3. The G-R parameter presents the highest CoV values, thus being the most dispersed criterion among the others. One of the reasons is the fact that the G-R parameter considers the complex modulus norm, whose conversion between  $|E^*|$  and  $|G^*|$  was made considering an approximate value of Poisson's ratio of 0.5. The other three criteria that are solely based on phase angle displayed relatively low

variations, which was expected since the phase angle master curves obtained with experimental data from Metravib DMA and DSR overlap each other satisfactorily, as shown in Figure 5. These results prove that the phase angle appears to be less impacted by the rheometer type and thus reinforcing the soundness of the phase angle as an evaluation tool to detect variations in the mechanical behavior of asphalt binder.

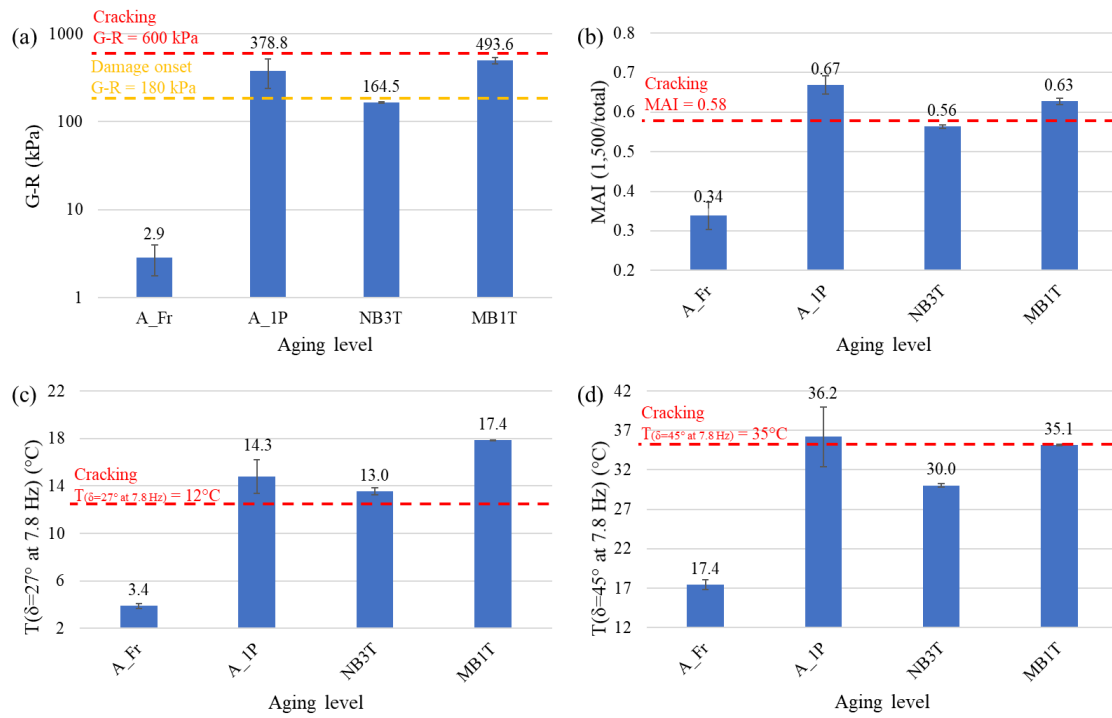


Figure 7. Rheology-based failure criteria and their corresponding thresholds: (a) G-R parameter, (b) MAI, (c)  $T(\delta=27^\circ \text{ at } 7.8 \text{ Hz})$ , and  $T(\delta=45^\circ \text{ at } 7.8 \text{ Hz})$ .

Table 3. Coefficient of variations of the G-R parameter,  $T_{(\delta=27^{\circ}\text{C at } 7.8 \text{ Hz})}$ ,  $T_{(\delta=27^{\circ}\text{C at } 7.8 \text{ Hz})}$ , and MAI of all the studied binders.

	<b>A_Fr</b>	<b>A_1P</b>	<b>NB3T</b>	<b>MB1T</b>
<b>G-R</b>	38.4%	36.9%	1.9%	8.4%
<b>T<sub>(<math>\delta=27^{\circ}</math> at 7.8 Hz)</sub></b>	6.5%	9.8%	2.4%	0.1%
<b>T<sub>(<math>\delta=45^{\circ}</math> at 7.8 Hz)</sub></b>	3.4%	10.4%	0.8%	0.3%
<b>MAI</b>	10.0%	3.4%	0.8%	1.3%

Figure 8 compares the AMWDs obtained through the  $\delta$ -method (left) and SEC with the 350 nm detector (right). The same trend can be observed in both cases where the AMWDs shift toward higher molecular weights. It is worth noting that the changes in the  $\delta$ -method AMWD curves with aging appear to emphasize the increase in the incidence of asphaltene molecular agglomeration through the new peak that emerges at around 2,000 g/mol. Despite their differences in shape and AMWD range, the AMWDs obtained by both methods are centralized at around 1,000 g/mol and present the same trend with AMWD obtained via SEC. When applying the concept of MAI to the AMWD curves obtained via SEC, a good relationship can be observed between the ELSD curves and MAI as presented in Figure 9 (left). Figure 9 (right) reveals that MAI is directly and indirectly proportional to the SAR-AD total saturates and total asphaltenes contents, respectively.

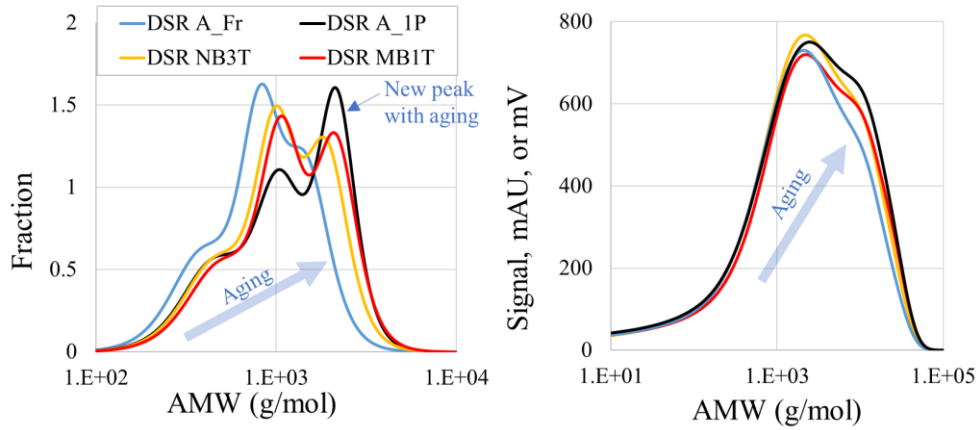


Figure 8. AMWDs with the  $\delta$ -method AMWD (left) and optical absorbance detector at 350 nm (right).

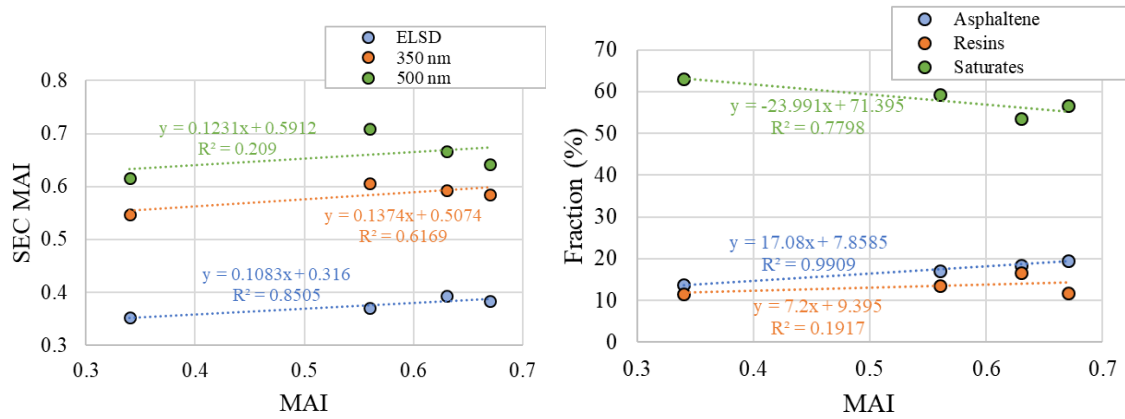


Figure 9. SEC MAI with ELSD and optical absorbance detector at 350 nm and 500 nm versus  $\delta$ -method MAI (left) and SAR-AD total aromatics, resins, and total asphaltenes contents versus MAI (right).

### 3 Conclusions

Based on the primary findings of this research work, the following conclusions can be drawn:

- The experimental and theoretical methods employed may provide valuable insights into binder aging since they have proved to be effective in assessing

binder chemistry and microstructure.

- SAR-AD showed that binder polarity and pericondensed aromaticity increase with aging, principally from the oxidation of aromatics 2 and 3 containing 2+ aromatic rings, which tend to decrease.
- SEC data from the 350 nm optical absorbance detector presents the overall AMWD curve, where a marked increase in the incidence of large molecular sizes is observed for less pericondensed aromatic molecules, essentially maltenes, with aging. On the other hand, 500 nm focuses on highly pericondensed asphaltenes, which also evolve under aging. This also shows the power of SEC when using proper detectors and conditions.
- As for the relatively new theoretical methods, both  $\delta$ -method and MAI, which are determined solely from rheology, satisfactorily corresponded with the SAR-AD and SEC results. This reinforces the soundness of both theoretical techniques to be used as a part of routine pavement evaluation testing to track cracking susceptibility of both laboratory- and field-aged binders.
- The satisfactory relationship observed between the experimental and theoretical methods opens encouraging perspectives towards a better understanding of how the changes in binder chemistry and microstructure affect binder performance.

### **Acknowledgments**

The authors gratefully acknowledge the French National Research Agency (ANR) funding this study under the MOVEDVDC project (ANR-17-CE22-0014). Also, the authors would like to thank Nadège Buisson (UGE), Christopher Seago (WRI), and Alex Literati (WRI) for providing the experimental data for the analyses presented in

this paper.

## References

- Adams, J. J., Elwardany, M. D., Planche, J.-P., Boysen, R. B., & Rovani, J. F. (2019). Diagnostic Techniques for Various Asphalt Refining and Modification Methods. *Energy & Fuels*. <https://doi.org/10.1021/acs.energyfuels.8b03738>
- Adams, J. J., Rovani, J. F., Boysen, R., Elwardany, M., & Planche, J.-P. (2021, June 15). *Innovations and developments in bitumen composition analysis*. 7th E&E congress, Madrid (online).
- Anderson, D. A., & Kennedy, T. W. (1993). Development of SHRP Binder Specification. *Journal of the Association of Asphalt Paving Technologists*, 62, 481–507.
- Booij, H. C., & Thoone, G. P. J. M. (1982). Generalization of Kramers-Kronig transforms and some approximations of relations between viscoelastic quantities. *Rheologica Acta*, 21(1), Article 1. <https://doi.org/10.1007/BF01520701>
- Boysen, R., & Schabron, J. (2015). *Automated HPLC SAR-AD Separation—Fundamental Properties of Asphalts and Modified Asphalts III Product: FP 01* (FP 01; Issue FP 01). Federal Highway Administration.
- Branthaver, J. F., Petersen, J. C., Robertson, R. E., Duvall, J. J., Kim, S. S., Harnsberger, P. M., Mill, T., Ensley, E. K., Barbour, F. A., & Schabron, J. F. (1993). *Binder Characterization and Evaluation Volume 2: Chemistry*. Strategic Highway Research Program, National Research Council.
- Chailleux, E., Ramond, G., Such, C., & de La Roche, C. (2006). A mathematical-based master-curve construction method applied to complex modulus of bituminous

- materials. *Road Materials and Pavement Design*, 7(sup1), Article sup1.  
<https://doi.org/10.1080/14680629.2006.9690059>
- Corbett, L. W. (1969). Composition of asphalt based on generic fractionation, using solvent deasphalting, elution-adsorption chromatography, and densimetric characterization. *Analytical Chemistry*, 41(4), Article 4.  
<https://doi.org/10.1021/ac60273a004>
- Groupe National Bitume. (1999). *Étude de la fissuration par le haut des bétons bitumineux: Suite de l'expérimentation "R.T.F.O.T"* (Laboratoire Central des Ponts et Chaussées, Ed.). Laboratoire central des ponts et chaussées.
- Hunter, R. N., Self, A., & Read, J. (2015). *The Shell Bitumen handbook* (Sixth edition). Published for Shell Bitumen by ICE Publishing.
- Krolkral, K., Haddadi, S., & Chailleux, E. (2018). Quantification of asphalt binder ageing from apparent molecular weight distributions using a new approximated analytical approach of the phase angle. *Road Materials and Pavement Design*, 21(4), Article 4. <https://doi.org/10.1080/14680629.2018.1536610>
- Lesueur, D., Elwardany, M. D., Planche, J.-P., Christensen, D., & King, G. N. (2021). Impact of the Asphalt Binder Rheological Behavior on the Value of the  $\Delta T_c$  Parameter. *Construction and Building Materials*, 293, 123464.  
<https://doi.org/10.1016/j.conbuildmat.2021.123464>
- Mullins, O. C. (2010). The Modified Yen Model. *Energy & Fuels*, 24(4), 2179–2207.  
<https://doi.org/10.1021/ef900975e>
- Mullins, O. C. (2011). The Asphaltenes. *Annual Review of Analytical Chemistry*, 4(1), Article 1. <https://doi.org/10.1146/annurev-anchem-061010-113849>
- Olard, F., & Di Benedetto, H. (2003). General “2S2P1D” Model and Relation Between the Linear Viscoelastic Behaviours of Bituminous Binders and Mixes. *Road*

*Materials and Pavement Design*, 4(2), Article 2.

<https://doi.org/10.1080/14680629.2003.9689946>

Petersen, J. C. (1984). Chemical Composition of Asphalt as Related to Asphalt Durability: State of the Art. *Transportation Research Record*, 999, Article 999.

Petersen, J. C. (2009). A Review of the Fundamentals of Asphalt Oxidation: Chemical, Physicochemical, Physical Property, and Durability Relationships.

*Transportation Research Circular, E-C140*, Article E-C140.

Pfeiffer, Ph., & Saal, R. N. J. (1940). Asphaltic Bitumen as Colloid System. *The Journal of Physical Chemistry*, 44(2), 139–149.

<https://doi.org/10.1021/j150398a001>

Rowe, G. M. (2011). Prepared discussion for the AAPT paper by Anderson et al.: Evaluation of the relationship between asphalt binder properties and non-load related cracking. *Journal of the Association of Asphalt Paving Technologists* 80, 80, 649–662.

Schabron, J. F., & Rovani, J. F. (2008). On-column precipitation and re-dissolution of asphaltenes in petroleum residua. *Fuel*, 87(2), Article 2.

<https://doi.org/10.1016/j.fuel.2007.04.024>

Siroma, R., Nguyen, M. L., Hornych, P., & Chailleux, E. (2022). A Literature Review of Bitumen Aging: From Laboratory Procedures to Field Evaluation. *Journal of Testing and Evaluation*, 50(2), 20210235. <https://doi.org/10.1520/JTE20210235>

Siroma, R. S., Nguyen, M. L., Hornych, P., Lorino, T., & Chailleux, E. (2021). Clustering aged bitumens through multivariate statistical analyses using phase angle master curve. *Road Materials and Pavement Design*, 22(sup1), Article sup1. <https://doi.org/10.1080/14680629.2021.1907217>

- Siroma, R. S., Nguyen, M. L., Hornych, P., Lorino, T., Hung, Y., Nicolai, A., Ziyani, L., & Chailleux, E. (2022). Molecular Agglomeration Index: Quantification of the Incidence of Asphaltene Molecular Agglomeration in Aged Asphalt Binders Through Rheological Measurements. *Transportation Research Record*, 15. <https://doi.org/10.1177/03611981221088597>
- Themeli, A., Chailleux, E., Farcas, F., Chazallon, C., & Migault, B. (2015). Molecular weight distribution of asphaltic paving binders from phase-angle measurements. *Road Materials and Pavement Design*, 16(sup1), Article sup1. <https://doi.org/10.1080/14680629.2015.1029667>
- Themeli, A., Marsac, P., Perez-Martinez, M., Krolkral, K., & Chailleux, E. (2016). A new method to quantify and evaluate ageing state of asphalt from viscoelastic measurement. *Proceedings of the International ISAP Symposium : From Molecules to Innovative Asphalt Pavements*, 14.
- Tuminello, W. H. (1986). Molecular weight and molecular weight distribution from dynamic measurements of polymer melts. *Polymer Engineering and Science*, 26(19), 1339–1347. <https://doi.org/10.1002/pen.760261909>
- Tuminello, W. H., & Cudré-Mauroux, N. (1991). Determining molecular weight distributions from viscosity versus shear rate flow curves. *Polymer Engineering & Science*, 31(20), Article 20. <https://doi.org/10.1002/pen.760312009>
- Williams, M. L., Landel, R. F., & Ferry, J. D. (1955). The Temperature Dependence of Relaxation Mechanisms in Amorphous Polymers and Other Glass-forming Liquids. *Journal of the American Chemical Society*, 77(14), Article 14. <https://doi.org/10.1021/ja01619a008>

Yen, T. Fu., Erdman, J. G., & Pollack, S. S. (1961). Investigation of the Structure of Petroleum Asphaltenes by X-Ray Diffraction. *Analytical Chemistry*, 33(11), 1587–1594. <https://doi.org/10.1021/ac60179a039>

Zanzotto, L., Stastna, J., & Ho, S. (1999). Molecular weight distribution of regular asphalts from dynamic material functions. *Materials and Structures*, 32(3), Article 3. <https://doi.org/10.1007/BF02481519>